A Redox-Active Two-Dimensional Coordination Polymer: Preparation of Silver and Gold Nanoparticles and Crystal Dynamics on Guest Removal

Myunghyun Paik Suh,* Hoi Ri Moon, Eun Young Lee, and Seung Yeon Jang

Contribution from the Department of Chemistry, Seoul National University, Seoul 151-747, Republic of Korea

Received October 12, 2005; Revised Manuscript Received February 13, 2006; E-mail: mpsuh@snu.ac.kr

Abstract: A two-dimensional (2D) square-grid coordination polymer, $\{[Ni(cyclam)]_2[BPTC]\}_n \cdot 2n H_2O$ (**1**), has been assembled from $[Ni(cyclam)](ClO_4)_2$ (cyclam = 1,4,8,11-tetraazacyclotetradecane) and H_4BPTC (H_4BPTC = 1,1′-biphenyl-2,2′,6,6′-tetracarboxylic acid) in $H_2O/MeOH$ (2.5:1, v/v) in the presence of triethylamine. When solid **1** was immersed in the EtOH solutions of $AgNO_3$ (1.3×10^{-1} M) and $NaAuCl_4 \cdot 2H_2O$ (3.4×10^{-2} M), respectively, for 5 min at room temperature, solids including Ag (3.7 ± 0.4 nm, diameter) and Au (2 nm, diameter) nanoparticles were formed by the redox reactions between Ni(II) ions incorporated in **1** and metal ions, as evidenced by HRTEM images, EPR, and XPS spectra. When single-crystal **1** was heated at 180 °C under 10^{-5} Torr for 24 h, it was transformed to dehydrated compound $\{[Ni(cyclam)]_2[BPTC]\}_n$ (**2**) in the single-crystal-to-single-crystal manner. The X-ray crystal structure of **2** reveals extensive dynamic motions of the molecular components in response to guest removal, involving rotation of the carboxylate and macrocycle, swing of the biphenyl, and bending of the macrocyclic coordination plane toward the carboxylate plane, which reduces the interlayer distance.

Introduction

Coordination polymers with open structure have attracted great attention[1−14] because they have potential as new materials that can be applied in selective molecular adsorption,[5−9] gas storage,[1,9,10] ion exchange,[11−13] and heterogeneous catalysis.[14,15] In particular, redox-active coordination polymers are useful because they can react with certain chemicals to produce oxidized frameworks and reduced substrates. Previously, we reported on a redox-active coordination polymer that reacted with I_2 to form an oxidized framework including I_3^- anions in the channels.[8] The coordination polymer retained its single crystallinity as well as its framework structure even after the redox reaction. We also reported that the redox-active coordination polymer produced silver nanoparticles of 3 nm, which had been known to be difficult to fabricate due to their strong tendency to aggregate,[16,17] upon immersion in the Ag(I) solution.[18]

Recently, flexible and dynamic coordination polymers, which can change their structures in response to external stimuli with retention of single crystallinity, have attracted growing interest[9,19−25] since they are important for the development of certain devices and sensors. We reported previously that the pillared bilayer network underwent spongelike shrinkage depending on the amount of guest molecules[7,8] and that the three-dimensional (3D) metal−organic framework with a PdF_2 net structure underwent rotational motion of the molecular components on desolvation with retention of single crystallinity.[19]

Here, we report a new redox-active two-dimensional (2D) square-grid coordination polymer, $\{[Ni(cyclam)]_2[BPTC]\}_n \cdot 2n H_2O$ (**1**). Solid **1** produces relatively monodispersed small

(1) Matsuda, R.; Kitaura, R.; Kitagawa, S.; Kubota, Y.; Belosludov, R. V.; Kobayashi, T. C.; Sakamoto, H.; Chiba, T.; Tanaka, M.; Kawazoe, Y.; Mita, Y. *Nature* **2005**, *436*, 238−240.
(2) Saied, O.; Maris, T.; Wuest, J. D. *J. Am. Chem. Soc.* **2003**, *125*, 14956−14957.
(3) Hagrman, P. J.; Hagrman, D.; Zubieta, J. *Angew. Chem., Int. Ed.* **1999**, *38*, 2638−2684.
(4) Duren, T.; Sarkisov, L.; Yaghi, O. M.; Snurr, R. Q. *Langmuir* **2004**, *20*, 2683−2689.
(5) Min, K. S.; Suh, M. P. *Chem. Eur. J.* **2001**, *7*, 303−313.
(6) Choi, H. J.; Lee, T. S.; Suh, M. P. *Angew. Chem., Int. Ed.* **1999**, *38*, 1405−1408.
(7) Suh, M. P.; Ko, J. W.; Choi, H. J. *J. Am. Chem. Soc.* **2002**, *124*, 10976−10977.
(8) Choi, H. J.; Suh, M. P. *J. Am. Chem. Soc.* **2004**, *126*, 15844−15851.
(9) Lee, E. Y.; Suh, M. P. *Angew. Chem., Int. Ed.* **2004**, *43*, 2798−2801.
(10) Rosi, N. L.; Eckert, J.; Eddaoudi, M.; Vodak, D. T.; Kim, J.; O'Keeffe, M.; Yaghi, O. M. *Science* **2003**, *300*, 1127−1129.
(11) Choi, H. J.; Suh, M. P. *Inorg. Chem.* **2003**, *42*, 1151−1157.
(12) Min, K. S.; Suh, M. P. *J. Am. Chem. Soc.* **2000**, *122*, 6834−6840.
(13) Tien, P.; Chau, L.-K.; Shieh, Y.-Y.; Lin, W.-C.; Wei, G.-T. *Chem. Mater.* **2001**, *13*, 1124−1130.
(14) Xu, Y.; Gu, W.; Gin, D. L. *J. Am. Chem. Soc.* **2004**, *126*, 1616−1617.
(15) Seo, J. S.; Whang, D.; Lee, H.; Jun, S. I.; Oh, J.; Jeon, Y. J.; Kim, K. *Nature* **2000**, *404*, 982−986.

(16) Wang, L.-Z.; Shi, J.-L.; Zhang, W.-H.; Ruan, M.-L.; Yu, J.; Yan, D.-S. *Chem. Mater.* **1999**, *11*, 3015−3017.
(17) Besson, S.; Gacoin, T.; Ricolleau, C.; Boilot, J.-P. *Chem. Commun.* **2003**, 360−361.
(18) Moon, H. R.; Kim, J. H.; Suh, M. P. *Angew. Chem., Int. Ed.* **2005**, *44*, 1261−1265.
(19) Lee, E. Y.; Jang, S. Y.; Suh, M. P. *J. Am. Chem. Soc.* **2005**, *127*, 6374−6381.
(20) Biradha, K.; Fujita, M. *Angew. Chem., Int. Ed.* **2002**, *41*, 3392−3395.
(21) Biradha, K.; Hongo, Y.; Fujita, M. *Angew. Chem., Int. Ed.* **2002**, *41*, 3395−3398.
(22) Kepert, C. J.; Rosseinsky, M. J. *Chem. Commun.* **1999**, 375−376.
(23) Takaoka, K.; Kawano, M.; Tominaga, M.; Fujita, M. *Angew. Chem., Int. Ed.* **2005**, *44*, 2151−2154.
(24) Wu, C.-D.; Lin, W. *Angew. Chem., Int. Ed.* **2005**, *44*, 1958−1961.
(25) Dybtsev, D. N.; Chun, H.; Kim, K. *Angew. Chem., Int. Ed.* **2004**, *43*, 5033−5036.

Ag and Au nanoparticles at room temperature simply upon immersion of the solids in Ag(I) and Au(III) solutions, respectively. This is the first report of the preparation of Au nanoparticles from Au(III) solution by using a coordination polymer solid without extra reducing agent. In addition, solid **1** undergoes a single-crystal-to-single-crystal transformation on removal of the guest water molecules intercalated between the layers, to furnish the desolvated crystal $\{[Ni(cyclam)]_2[BPTC]\}_n$ (**2**). The X-ray crystal structure of **2** reveals, for the fist time, that various types of motions of the molecular components are involved in the reduction of the interlayer distance on desolvation, such as rotation of the carboxylate and macrocycle, swing of the biphenyl, and bending of the macrocyclic coordination plane toward the carboxylate plane. Although crystal dynamics involving spongelike shrinkage/swelling,[7,8,23] sliding,[20,21] swing,[25] or rotation[19] have been independently reported, those involving various types of motions have never been observed.

Experimental Section

General. All chemicals and solvents used in the syntheses were of reagent grade and were used without further purification. H₄BPTC (1,1′-biphenyl-2,2′,6,6′-tetracarboxylic acid) and [Ni(cyclam)](ClO₄)₂ were prepared according to the methods previously reported.[26,27] NMR spectra were measured on a Bruker Spectrospin 300. Infrared spectra were recorded on a PerkinElmer FT-IR Spectrum One spectrophotometer. UV/vis diffuse reflectance spectra were recorded on a PerkinElmer Lambda35 UV/vis spectrophotometer. EPR spectra were recorded on a Bruker EPR EMX spectrometer. Elemental analyses were performed in the analytical laboratory at Seoul National University. ICP-AES measurements were performed with a Shimadzu model ICPS-1000IV instrument. Thermogravimetric analysis (TGA) and differential scanning calorimetry (DSC) were performed under N₂ at a scan rate of 5 °C/min using a Q50 and a Q10 from TA Instruments, respectively. Gas sorption data were measured by static volumetric method on a Quantachrome Autosorb-1 gas sorption apparatus. X-ray powder diffraction (XRPD) data were recorded on a Bruker D5005 diffractometer at 40 kV and 40 mA for Cu Kα ($\lambda = 1.54050$ Å) with a scan speed of 2°/min and a step size of 0.02° in 2θ. X-ray photoelectron spectra were measured on a Sigma Probe. HRTEM images were obtained on a JEOL JEM-3000F microscope.

Preparation of H₄BPTC·Pyridine·MeOH. H₄BPTC (4.70 g, 14.2 mmol) was dissolved in hot MeOH (100 mL), and then pyridine (7 mL) was added. The solution was allowed to stand at room temperature for 1 day until colorless crystals formed, which were filtered off, washed with MeOH, and dried in vacuo. Yield: 4.63 g (74%). Anal. Calcd for C₂₂H₁₉NO₉: C, 59.86; H, 4.34; N, 3.17. Found: C, 59.25; H, 3.94; N, 3.09. ¹H NMR (D₂O): $\delta = 8.72-8.70$ (d, 2H), 8.58–8.52 (t, 1H), 8.03–7.95 (t, 2H), 7.71–7.68 (d, 4H), 7.57–7.52 (t, 2H).

Preparation of $\{[Ni(cyclam)]_2[BPTC]\}_n \cdot 2nH_2O$ (1). To a hot H₂O/MeOH (2.5 mL/1 mL) solution of [Ni(cyclam)](ClO₄)₂ (0.189 g, 0.53 mmol) was added a hot H₂O/MeOH/TEA (2.5 mL/1 mL/0.24 mL) solution of H₄BPTC·pyridine·MeOH (0.125 g, 0.28 mmol). The reaction vessel was tightly closed, and the solution was allowed to stand at 35 °C for 3 days until purple crystals formed, which were filtered off, washed with a mixture of H₂O and MeOH, and dried in air. Yield: 0.157 g (70%). Anal. Calcd for Ni₂C₃₆H₅₈N₈O₁₀: C, 49.12; H, 6.64; N, 12.73. Found: C, 49.63; H, 6.72; N, 12.82. FT-IR (KBr pellet): $\nu_{OH(water)}$, 3464 (m, br); ν_{NH}, 3264, 3208, 3137 (m, split); ν_{CH_2}, 2934 (s), 2851 (s); $\nu_{O-C=O}$, 1569 (s), 1557 (s) cm⁻¹. UV/vis (diffuse reflectance spectrum, λ_{max}): 516 nm.

(26) Pryor, K. E.; Shipps, G. W., Jr.; Skyler, D. A.; Rebek, J., Jr. *Tetrahedron* **1998**, *54*, 4107−4124.
(27) Barefield, E. K.; Bianchi, A.; Billo, E. J.; Conolly, P. J.; Paoletti, P.; Summers, J. S.; Vanderveer, D. G. *Inorg. Chem.* **1986**, *25*, 4197−4202.

$\{[Ni(cyclam)]_2[BPTC]\}_n$ (2). A single crystal of **1** was introduced into a 0.5 mm glass capillary having an open end, which was inserted into a 12 mm cell and then heated at 180 °C under 10⁻⁵ Torr for 24 h on a Quantachrome Autosorb-1 instrument. After the cell was cooled to room temperature under vacuum and then filled with He gas (1.0 atm), the capillary was taken out and sealed immediately for the X-ray diffraction measurements. For preparation of bulk amount of **2**, solid **1** (98 mg) was heated in a Schlenk tube at 180 °C under vacuum for 3 h. Anal. Calcd for Ni₂C₃₆H₅₄N₈O₈: C, 51.22; H, 6.44; N, 13.27. Found: C, 50.57; H, 6.38; N, 13.40. FT-IR (Nujol mull): ν_{NH}, 3265, 3202, 3130 (m); ν_{CH_2}, 2923 (s), 2854 (s); $\nu_{O-C=O}$, 1575, 1554 (s, split) cm⁻¹. UV/vis (diffuse reflectance spectrum, λ_{max}): 516 nm.

Gas Sorption Study. A measured amount of $\{[Ni(cyclam)]_2[BPTC]\}_n \cdot 2nH_2O$ (**1**) was introduced into a Quantachrome Autosorb-1 gas sorption apparatus, and then the compound was evacuated at 180 °C and 10⁻⁵ Torr to remove all guest water molecules. The nitrogen gas sorption isotherm was monitored at 77 K at each equilibrium pressure by the static volumetric method.

Preparation of Ag Nanocomposites. Solid **1** (0.067 g, 0.076 mmol) was ground into a powder and then immersed at room temperature for 5 min to 16 h in the EtOH solution (3 mL) of AgNO₃ (1.3×10^{-1} M, 0.38 mmol), which was prepared by sonicating the AgNO₃ solid in EtOH. A dark brown solid resulted, and the color of the solution became pale yellow, indicating partial dissociation of the Ni(II)−cyclam complex from **1**. The solid was filtered off, washed with EtOH, and dried in air. Anal. Calcd for the solid isolated after 5 min of immersion, $\{[Ni^{III}(cyclam)]_2[BPTC]\}(NO_3)_2 \cdot 2Ag^0 \cdot H_2O \cdot 0.5Ag_4BPTC$ (Ni₂C₄₄H₅₉N₁₀O₁₉Ag₄): C, 33.43; H, 3.76; N, 8.86. Found: C, 32.97; H, 3.78; N, 8.85. ICP data (in HNO₃): concentration ratio of Ag/Ni = 154/41.3; mol ratio of Ag/Ni = 2.02. FT-IR (KBr pellet): 3429 (m, br), 3267, 3210, 3158 (m, split), 2927 (m), 2855 (m), 1567 (s), 1557 (s), 1463, 1446 (m, split), 1376 (s) cm⁻¹.

To see the concentration effect on the formation of nanoparticles, similar experiments were performed in more dilute EtOH solutions (1.0×10^{-2} and 4.0×10^{-3} M) of AgNO₃. To see the temperature effect, the experiment was performed in boiling EtOH solution. To see the solvent effect, the experiments were also carried out in a MeOH solution of AgNO₃ and in a toluene solution of AgCF₃SO₃ at room temperature. The results are presented in the Supporting Information.

Preparation of Au Nanocomposites. Solid **1** (0.069 g, 0.078 mmol) was ground into a powder and then immersed in the EtOH solution (6 mL) of NaAuCl₄·2H₂O (3.4×10^{-2} M, 0.20 mmol) at room temperature for 5 min to 46 h, respectively. The resulting brownish yellow powder was filtered off, washed with EtOH, and dried in air. Anal. Calcd for the solid isolated after 5 min of immersion, $[Ni^{III}(cyclam)]_2[BPTC] \cdot 2Cl^- \cdot ^2/_3Au^0 \cdot H_2O$ (Ni₂C₃₆H₅₆N₈O₉Au₀.₆₇Cl₂): C, 40.62; H, 5.30; N, 10.53. Found: C, 43.07; H, 5.65; N, 11.33. ICP data could not be obtained since gold oxide precipitated when the nanocomposite solid was dissolved in HCl. FT-IR (KBr pellet): 3430 (m, br), 3264, 3211, 3148 (m, split), 2926 (m), 2858 (m), 1592 (s), 1574 (s), 1555 (s), 1464, 1455, 1429 (m, split), 1373 (s) cm⁻¹.

To see the concentration effect on the formation of nanoparticles, similar experiments were performed in EtOH solutions of NaAuCl₄·2H₂O with different concentrations, 1.6×10^{-3} and 3.01×10^{-1} M, at room temperature. To see the temperature effect, the same experiments were performed in boiling EtOH solutions. To see the solvent effect, the experiments were also carried out in MeCN solution at room temperature. The results are provided in the Supporting Information.

Crystallography. Diffraction data for **1** and **2** were collected with an Enraf Nonius Kappa CCD diffractometer (Mo Kα, $\lambda = 0.71073$ Å, graphite monochromator). Preliminary orientation matrices and unit cell parameters were obtained from the peaks of the first 10 frames and then refined using the whole data set. Frames were integrated and corrected for Lorentz and polarization effects using DENZO.[28] The scaling and the global refinement of the crystal parameters were performed by using SCALEPACK.[28] No absorption correction was

Table 1. Crystallographic Data for **1** and **2**

	compound	
	1	**2**
formula	$Ni_2C_{36}H_{58}N_8O_{10}$	$Ni_2C_{36}H_{54}N_8O_8$
crystal system	triclinic	triclinic
space group	$P\bar{1}$	$P\bar{1}$
fw	880.3	844.3
a, Å	11.9228(5)	12.2254(9)
b, Å	12.6428(6)	12.3221(10)
c, Å	14.7501(7)	14.6164(10)
α, deg	73.718(2)	67.236(4)
β, deg	77.317(3)	73.364(4)
γ, deg	77.917(3)	77.756(4)
V, Å^3	2063.7(14)	1932.5(2)
Z	2	2
ρ_{calcd}, g cm^{-3}	1.422	1.451
temp, K	293(2)	293(2)
λ, Å	0.71073	0.71073
μ, mm^{-1}	0.980	1.035
goodness-of-fit (F^2)	1.070	1.049
$F(000)$	932	892
reflections collected	13 604	11 718
independent reflections	9370	8743
	[R(int) = 0.0460]	[R(int) = 0.0312]
completeness to θ_{max}, %	99.6	98.5
data/parameters/restraints	9370/501/8	8743/517/8
crystal size, mm^3	0.3 × 0.2 × 0.1	0.3 × 0.2 × 0.1
θ range for data collection, deg	1.46−27.46	1.55−27.52
diffraction limits	−14 ≤ h ≤ 15	−15 ≤ h ≤ 15
(h, k, l)	−16 ≤ k ≤ 13	−15 ≤ k ≤ 16
	−19 ≤ l ≤ 19	−13 ≤ l ≤ 18
refinement method	full-matrix least squares on F^2	full-matrix least squares on F^2
R_1, wR_2 [$I > 2\sigma(I)$]	0.0724,^{a} 0.2061^b	0.0565,^{a} 0.1437^c
R_1, wR_2 (all data)	0.1719,^{a} 0.2776^b	0.1338,^{a} 0.2094^c
largest peak, hole, e·Å^{-3}	1.148, −0.917	0.825, −0.899

^{a} $R = \sum||F_o| - |F_c||/\sum|F_o|$. ^{b} $wR(F^2) = [\sum w(F_o^2 - F_c^2)^2/\sum w(F_o^2)^2]^{1/2}$, where $w = 1/[\sigma^2(F_o^2) + (0.1455P)^2 + 0.6236P]$, $P = (F_o^2 + 2F_c^2)/3$ for **1**. ^{c} $wR(F^2) = [\sum w(F_o^2 - F_c^2)^2/\sum w(F_o^2)^2]^{1/2}$, where $w = 1/[\sigma^2(F_o^2) + (0.1023P)^2 + 1.8896P]$, $P = (F_o^2 + 2F_c^2)/3$ for **2**.

made. The crystal structures were solved by direct methods[29] and refined by full-matrix least-squares refinement using the SHELXL-97 computer program.[30] The positions of all non-hydrogen atoms were refined with anisotropic displacement factors. The hydrogen atoms, except those on the nitrogen atom, were positioned geometrically and refined using a riding model. A water molecule per formula unit of the host was refined, which was disordered at two close sites with half occupancy. The crystallographic data are summarized in Table 1.

Results and Discussion

Preparation and X-ray Crystal Structure of {[Ni(cyclam)]$_2$-[BPTC]}$_n$·2nH$_2$O (1). Our design strategy was to build a 2D square-grid network by utilizing BPTC^{4-} and a Ni(II) macrocyclic complex (Scheme 1). We chose BPTC^{4-} as the planar four-connecting organic building block because the X-ray structure of H$_4$BPTC revealed approximately perpendicular orientation of its phenyl rings (86.3°).[31] We employed Ni(II)−cyclam complex as a linear metal building block because it contains two vacant coordination sites at the axial sites.[5−11,18]

(28) Otwinowsky, Z.; Minor, W. In *Processing of X-ray Diffraction Data Collected in Oscillation Mode*; Carter, C. W., Jr., Sweet, R. M., Eds.; Methods in Enzymology 276; Academic Press: San Diego, CA, 1996; pp 307−326.
(29) Sheldrick, G. M. *Acta Crystallogr.* **1990**, *A46*, 467.
(30) Sheldrick, G. M. *SHELXL97, Program for the crystal structure refinement*; University of Göettingen: Göettingen, Germany, 1997.
(31) Holy, P.; Zavada, J.; Cisarova, I.; Podlaha, J. *Angew. Chem., Int. Ed.* **1999**, *38*, 381−383.

Scheme 1

Furthermore, Ni(II)−cyclam complex, coordinating anionic ligands at the axial sites, can be oxidized to Ni(III) species by using the appropriate oxidizing agents.[8,18,32]

The self-assembly of Ni(II)−cyclam complex and BPTC^{4-} afforded {[Ni(cyclam)]$_2$[BPTC]}$_n$·2nH$_2$O (**1**). Solid **1** is soluble in hot water but insoluble in common organic solvents such as MeOH, EtOH, MeCN, benzene, dimethyl sulfoxide, diethyl-formamide, and dimethylformamide. Thermogravimetric analysis (TGA) of **1** shows weight loss of 4.1% at 20−315 °C (see Supporting Information), which corresponds to the loss of two water guest molecules per formula unit (calcd 4.1%). Differential scanning calorimetry (DSC) indicates that **1** loses one water molecule at ca. 100 °C and the other at ca. 250 °C. The host is thermally stable up to 330 °C.

The X-ray crystal structure of **1** is shown in Figure 1. Each BPTC^{4-} coordinates four Ni(II) macrocyclic complexes, and each Ni(II) macrocyclic complex binds two oxygen atoms of two different BPTC^{4-} ligands at the axial sites, which results in a 2D square-grid network. Every noncoordinating carbonyl oxygen atom of BPTC^{4-} interacts with the N−H of the macrocycle to form a hydrogen-bonded six-membered ring. Two phenyl rings of a BPTC^{4-} are twisted almost perpendicularly with respect to each other (dihedral angle, 77.9(2)°), and the line connecting the C4··C1−C7··C10 atoms of BPTC^{4-} becomes a pseudo-two-fold rotational axis. Each square compartment of the square grid, which consists of four Ni(II) macrocyclic complexes and four BPTC^{4-} anions, is chiral because it possesses quasi-D_4 symmetry (Figure 2a). The size of the square compartment is 10 Å × 11 Å, but the effective void size is ca. 1 Å. The chirality of the square compartments in a 2D network occurs alternately in the horizontal and vertical rows, and thus the infinite layer becomes achiral (Figure 2b). The 2D grid forms an uneven plane of ca. 1 nm thickness because of the macrocycles and phenyl rings of BPTC^{4-}. The 2D layers extend parallel to the (110) plane and are stacked in a staggered manner with respect to the chirality of the square compartments (Figure 2c). Although the elemental analysis and TGA/DSC data indicate that the network contains two water guest molecules per formula unit, the X-ray crystal structure defines only one water molecule that is disordered in two parts. The refined water guest molecules locate between the layers instead of inside the square compartments. The void volume in **1** is about 12% of the total crystal volume, as estimated by using PLATON.[33]

Redox Reaction of Solid 1 with the Ag(I) Solution. When pale purple solid **1** was immersed in the EtOH solution of AgNO$_3$ (1.3 × 10^{-1} M) at room temperature for 5 min, the color of **1** changed immediately to brown and Ag nanoparticles

(32) Suh, M. P. *Advances in Inorganic Chemistry*; Academic Press: New York, 1997; Vol. 44, pp 93−146.
(33) Spek, A. L. *PLATON99, A Multipurpose Crystallographic Tool*; Utrecht University: Utrecht, The Netherlands, 1999.
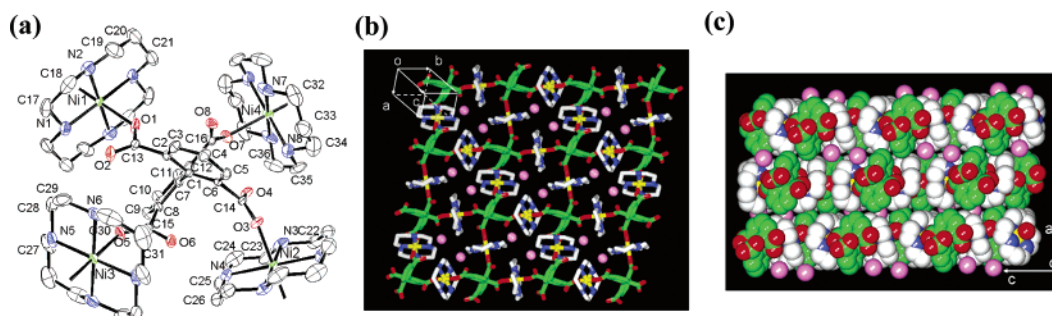
Figure 1. X-ray crystal structure of $\{[Ni(cyclam)]_2[BPTC]\}_n \cdot 2nH_2O$ (**1**). (a) An ORTEP drawing of **1** with atomic numbering scheme. The thermal ellipsoids are drawn with 30% probability. (b) Top view seen on the (110) plane, showing the 2D square-grid network. (c) Side view (in CPK) showing the stacking of the 2D layers. Ni, yellow; O(BPTC), red; N, blue; C(cyclam), white; C(BPTC), green; guest water, pink.
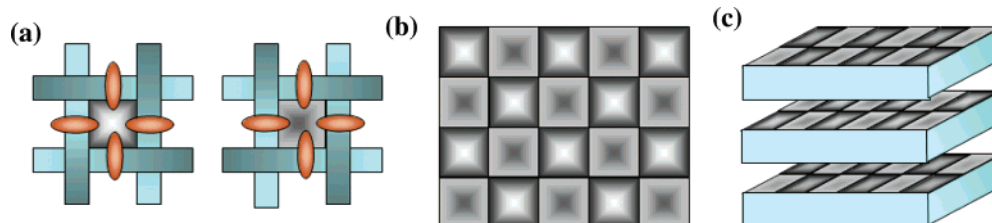

Figure 2. Schematic diagrams for the X-ray structure of **1**. (a) Two different chiral square compartments. (b) An achiral square-grid network constructed of square compartments having different chirality. Different chirality is indicated by different shading. (c) Stacking mode of 2D layers in the ABAB sequence.
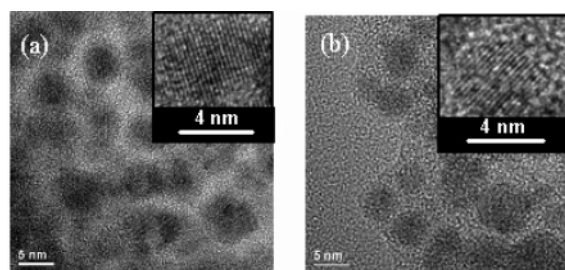

Figure 3. HRTEM images of Ag nanoparticles formed by immersion of solid **1** in the EtOH solution of $AgNO_3$ (1.3×10^{-1} M) at room temperature (a) for 5 min and (b) for 16 h.

Figure 4. EPR spectrum of the host solid (powder sample) isolated after immersion of **1** in the EtOH solution of $AgNO_3$ (1.3×10^{-1} M) for 5 min. Measured at room temperature; $g_\perp = 2.198$ and $g_{\parallel} = 2.028$.

(3.7 ± 0.4 nm diameter) were formed, as shown in Figure 3. The color change of the host solid must be attributed to the oxidation of Ni(II) ions incorporated in the host to the Ni(III) state[18,32] by Ag(I) ions as well as the surface plasma formed by Ag nanoparticles.[34,35] The size of the Ag nanoparticles did not change even after immersion of solid **1** in the $AgNO_3$ solution for 16 h.

It has been known that Ag(I) ions can be reduced in alcoholic solutions in the presence of stabilizers with an extra stimulus such as microwave, laser, UV light, or chemical reducing agents.[36] However, the yield of Ag nanoparticles (3−10 nm) formed from the EtOH solution of $AgNO_3$ is less than 1%, even in the presence of nonionic surfactant and at high temperature, where the formation rate increased with increasing Ag(I) salt concentration and temperature.[37] It has been also known that
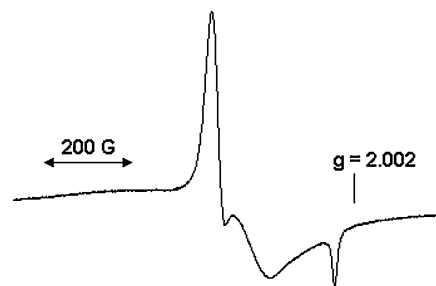
preparation of Ag nanoparticles smaller than 5 nm is much more difficult than that of Au or Pt nanoparticles because of the strong tendency of Ag particles to aggregate.[17]

In this study, Ag nanoparticles of ca. 4 nm were obtained by the simple immersion of **1** in the $AgNO_3$ solution for 5 min at room temperature. The solid includes free NO_3^- ions, as shown by a peak at 1383 cm^{-1} in the IR spectrum, since the host solid including Ag nanoparticles becomes positively charged due to the redox reaction with Ag(I) ion.

The EPR spectrum (Figure 4) of the resulting solid shows anisotropic signals at $g_\perp = 2.198$ and $g_{\parallel} = 2.028$, indicative of the tetragonally distorted Ni(III) species.[18,32,38] Even though the EPR spectrum does not show a Ag(0) peak, which is known to appear at $g \approx 1.966-2.043$,[39,40] the X-ray photoelectron spectra (XPS) as well as the energy-dispersive X-ray spectroscopy (EDS) data indicate that Ag(0) and Ni(III) coexist in the solid (Figure 5 and Supporting Information). In the XPS, the $3d_{5/2}$ and $3d_{3/2}$ peaks for Ag(0) appear at 368.6 and 374.6 eV, respectively, which are coincident with the reported values (368

(34) Korchev, A. S.; Bozack, M. J.; Slaten, B. L.; Mills, G. *J. Am. Chem. Soc.* **2004**, *126*, 10−11.
(35) Kelly, K. L.; Coronado, E.; Zhao, L.; Schatz, G. C. *J. Phys. Chem. B* **2003**, *107*, 668−677.
(36) (a) He, R.; Qian, X.; Yin, J.; Zhu, Z. *J. Mater. Chem.* **2002**, *12*, 3783−3786. (b) Yamamoto, T.; Wada, Y.; Sakata, T.; Mori, H.; Goto, M.; Hibino, S.; Yanagida, S. *Chem. Lett.* **2004**, *33* (2), 158−159. (c) Abid, J. P.; Wark, A. W.; Brevet, P. F.; Girault, H. H. *Chem. Commun.* **2002**, 792−793. (d) Itakura, T.; Torigoe, K.; Esumi, K. *Langmuir* **1995**, *11*, 4129−4134. (e) Petit, C.; Lixon, P.; Pileni, M.-P. *J. Phys. Chem.* **1993**, *97*, 12974−12983.
(37) Liz-Marzan, L. M.; Lado-Tourino, I. *Langmuir* **1996**, *12*, 3585−3589.
(38) Suh, M. P.; Lee, E. Y.; Shim, B. Y. *Inorg. Chim. Acta* **1998**, 337−341.
(39) Yamada, H.; Michalik, J.; Sadlo, H.; Perlinska, J.; Takenouchi, S.; Shimomura, S.; Uchida, Y. *Appl. Clay Sci.* **2001**, *19*, 173−178.
(40) Michalik, J.; Kevan, L. *J. Am. Chem. Soc.* **1986**, *108*, 4247−4253.
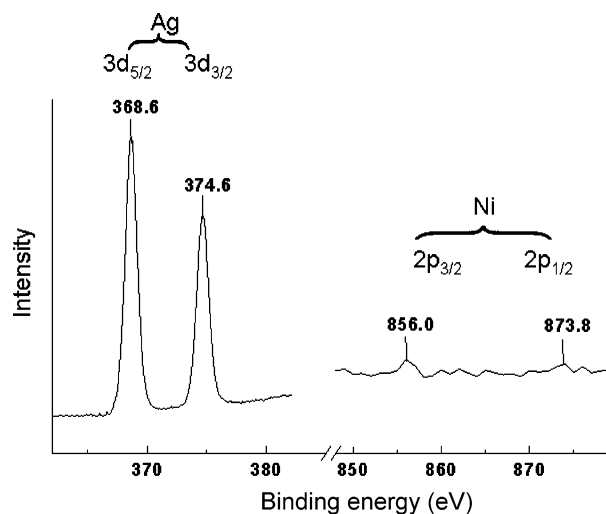
Figure 5. X-ray photoelectron spectrum for the solid isolated after **1** was immersed in the EtOH solution of AgNO$_3$ (1.3×10^{-1} M) for 5 min.

Figure 6. XRPD patterns for (a) original host framework **1**, (b) solid isolated after immersion of solid **1** in the EtOH solution of AgNO$_3$ (1.3×10^{-1} M) for 5 min, (c) solid isolated after immersion for 20 min, (d) solid isolated after immersion for 60 min, and (e) solid isolated after immersion for 16 h.

and 374 eV) for the metallic Ag,[41,42] and 2p$_{3/2}$ and 2p$_{1/2}$ peaks for Ni(III) appear at 856.0 and 873.8 eV, respectively, which are similar to those (853 and 870 eV) for the Ni(III) ions in the inorganics.[43] Although the Ni(III) species is in an uncommon oxidation state, it can be stabilized by the presence of an azamacrocyclic ligand in a pseudo-octahedral species with anionic axial ligands.[8,18,32,38]

In general, the size, shape, and crystallinity of the nanoparticles depend on the concentration of metal ions, the temperature, and the type of solvent.[36a,44] In this study, we carried out the experiments under various experimental conditions: metal ion concentration, $4.0 \times 10^{-3}-1.3 \times 10^{-1}$ M; temperature, room temperature to 78.5 °C; solvent, EtOH, MeOH, and toluene. The results indicate that the concentration of Ag(I) salt, the temperature, and the type of solvent do not significantly affect the size of the nanoparticles (see Supporting Information). When the same reaction was performed in MeOH, where host **1** was insoluble, Ag nanoparticles (ca. 4 nm) were also formed, but [Ni(cyclam)]$^{2+}$ species incorporated in the layer were dissociated into the solution.

To see if the silver nanoparticles were formed only by the Ni(II) macrocyclic complex, Ni(II) macrocyclic complexes coordinated with various carboxylate ligands, such as benzoate, 4-biphenylcarboxylate, and 2-naphthalenecarboxylate, were prepared to make the coordination environment of the Ni(II) species similar to that in **1**. Since only the complex coordinating 2-naphthalenecarboxylate was insoluble in EtOH, solid [Ni(cyclam)(2-naphthalenecarboxylate)$_2$] (0.056 g, 0.084 mmol) was immersed in the EtOH solution of AgNO$_3$ (4.2×10^{-3} M, 50 mL, 0.21 mmol) for 5 min. The pink solid became a fibrous gray material, and its TEM image showed formation of silver particles (7−22 nm) much bigger than those formed by solid **1** (see Supporting Information). The IR spectra and EDS data
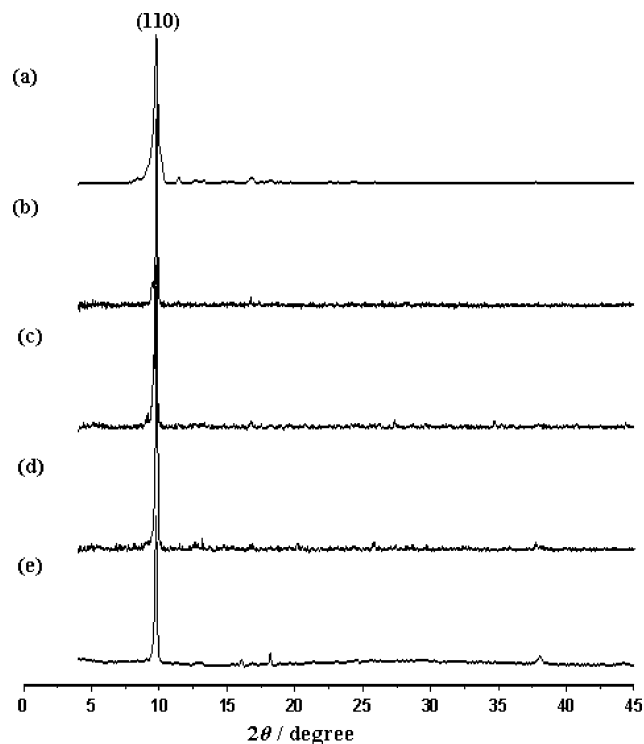
indicate that the solid contains no macrocyclic complex. The EPR spectrum of the solid, which is inactive, also indicates that no Ni(III)−cyclam species exists in the solid. It seems that [Ni(cyclam)(2-naphthalenecarboxylate)$_2$] dissociates in the EtOH solution of AgNO$_3$, and 2-naphthalenecarboxylate forms a Ag(I) salt, which must be reduced to Ag particles. The results suggest that both the open structure and the redox-active Ni(II) macrocyclic component are necessary to obtain the monodispersed and small (ca. 4 nm) Ag nanoparticles.

The XRPD patterns (Figure 6) indicate that the network structure of **1** is retained even after Ag nanoparticles (ca. 4 nm) are formed by the immersion of solid **1** in the AgNO$_3$ solution for 5 min to 16 h. The peaks corresponding to crystalline Ag structure generally appear at $2\theta = 38.1°$ and $44.2°$,[45] but their intensities in Figure 6 are weak, probably because the nanoparticles are too small. It should be emphasized here that the structure of the square-grid network is maintained even when the Ni(II) species of the network are oxidized to Ni(III) by the Ag(I) ions, which results in the positively charged network intercalating NO$_3^-$ anions. Previously, we reported that the pillared-bilayer framework incorporating Ni(II) bismacrocyclic complexes retained its single crystallinity as well as the framework structure even after oxidation with I$_2$, which resulted in an oxidized framework containing Ni(III) species with I$_3^-$ inclusions in the channels.[8] The X-ray structure of the oxidized pillared-bilayer framework indicated that Ni(III)−ligand bond distances became shortened compared with Ni(II)−ligand distances, but this did not affect the integrity of the framework.

(41) Wagner, C. D. *Handbook of X-ray Photoelectron Spectroscopy, A Reference Book of Standard Data for Use in X-ray Photoelectron Spectroscopy*; Muilenberg, G. E., Ed.; Perkin-Elmer Corp.: Eden Prairie, MN, 1979.
(42) Yue, Z. R.; Jiang, W.; Wang, L.; Toghiani, H.; Gardner, S. D.; Pittman, C. U., Jr. *Carbon* **1999**, *37*, 1607−1618.
(43) Davidson, A.; Tempere, J. F.; Che, M. *J. Phys. Chem.* **1996**, *100*, 4919−4929.
(44) (a) Huang, H. H.; Ni, X. P.; Loy, G. L.; Chew, C. H.; Tan, K. L.; Loh, F. C.; Deng, J. F.; Xu, G. Q. *Langmuir* **1996**, *12*, 909−912. (b) Yamada, M.; Nishihara, H. *Langmuir* **2003**, *19*, 8050−8056. (c) Lu, L.; Wang, H.; Zhou, Y.; Xi, S.; Zhang, H.; Hu, J.; Zhao, B. *Chem. Commun.* **2002**, 144−145.

(45) (a) Han, Y.-J.; Kim, J. M.; Stucky, G. D. *Chem. Mater.* **2000**, *12*, 2068−2069. (b) Adhyapak, P. V.; Karandikar, P.; Vijayamohanan, K.; Athawale, A. A.; Chandwadkar, A. J. *Mater. Lett.* **2004**, *58*, 1168−1171.
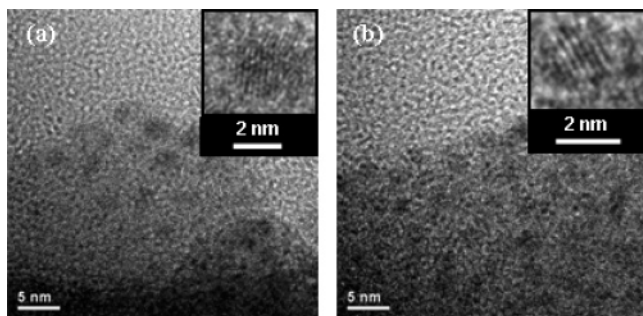
Figure 7. HRTEM images for the solid isolated after solid **1** was immersed in the EtOH solution of NaAuCl$_4$·2H$_2$O (3.4×10^{-2} M) at room temperature (a) for 5 min and (b) for 46 h.

It seems that the framework incorporating the Ni(II) macrocyclic species is so stable to the redox reaction that the structure can be retained even after the redox reaction.

The elemental analysis data (Experimental Section) indicate that a stoichiometric amount of Ag nanoparticles was formed by the 1:1 redox reaction between Ni(II) and Ag(I), which resulted in a positively charged network incorporating Ni(III) species with NO$_3^-$ inclusions. The data also imply that Ag$_4$BPTC salt precipitated and mixed with the nanocomposite, because solid **1** was partially dissociated in the AgNO$_3$ solution, as noted in the Experimental Section.

On the basis of the XRPD and EA data as well as EPR, XPS, and TEM results, we would suggest that Ag(I) metal ions are introduced between the host layers and react with the Ni(II) species incorporated in the host to form Ag(0) atoms, which diffuse to the surface of the solid to grow into nanoparticles. Since the Ag nanoparticles grew on the surface of the solid, the host structure could be maintained even after the nanoparticles of ca. 4 nm were formed. If the nanoparticles grew between the layers, the (110) peak of the XRPD should have shifted to the lower angle region. In addition, if the reduction of Ag(I) ions occurred only on the surface of the solid and aggregated to the nanoparticles, a much less than stoichiometric amount of nanoparticles should have formed. It should be noted that the void size cannot be related to the size of the nanoparticles in the present 2D square-grid network, because even the water guest molecules in **1** are intercalated between the layers instead of within the cavities of the square compartments (effective void size, ca. 1 Å).

Redox Reaction of Solid 1 with AuCl$_4^-$. When solid **1** was immersed in the EtOH solution of NaAuCl$_4$·2H$_2$O (3.4×10^{-2} M) at room temperature for 5 min, the color of the host solid immediately changed from pale purple to brownish yellow. There was no indication of the dissociation of Ni(II) macrocyclic complex from **1**. The HRTEM image of the solid that was isolated after immersion in the Au(III) solution for 5 min shows the formation of Au nanoparticles (ca. 2 nm diameter; Figure 7). Even when the solid was immersed for 46 h, the size and shape of the nanoparticles did not change.

The EPR spectrum of the resulting solid shows anisotropic signals at $g_\perp = 2.177$ and $g_\parallel = 2.026$, corresponding to the tetragonally distorted Ni(III) species (Figure 8),[18,32,38] indicating that a redox reaction occurred between the host and Au(III) ions. X-ray photoelectron and energy-dispersive X-ray spectroscopic data indicate that Au(0) and Ni(III) coexist in the solid (Figure 9 and Supporting Information). The peaks for Au(0), 4f$_{7/2}$ and
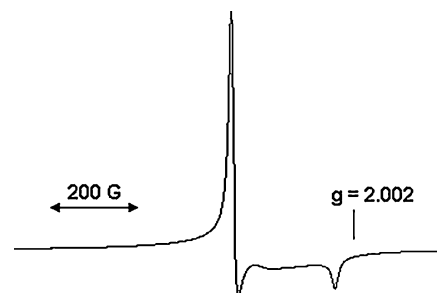

Figure 8. EPR spectrum of the solid (powder sample) isolated after solid **1** was immersed in the EtOH solution of NaAuCl$_4$·2H$_2$O (3.4×10^{-2} M) for 20 min. Measured at 102 K; $g_\perp = 2.177$ and $g_\parallel = 2.026$.

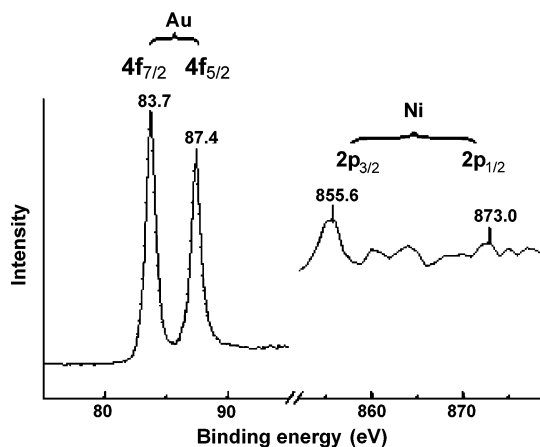**Figure 9.** X-ray photoelectron spectrum for the solid isolated after solid **1** (powder sample) was immersed in the EtOH solution of NaAuCl$_4$·2H$_2$O (3.4×10^{-2} M) for 5 min. Measured at room temperature.

4f$_{5/2}$, are observed at 83.7 and 87.4 eV, respectively, similar to the values (84 and 88 eV) reported for the metallic Au.[41,42] The peaks for Ni(III), 2p$_{3/2}$ and 2p$_{1/2}$, are observed at 855.6 and 873.0 eV, respectively, which are coincident with those (853 and 870 eV) for the Ni(III) ions in inorganics.[43]

The size of the Au nanoparticles was affected by the concentration of Au(III) solutions (1.6×10^{-3}–3.0×10^{-1} M in EtOH), but not by the immersion time (5 min–46 h), temperature (room temperature to 78.5 °C), and type of solvent (EtOH and MeCN), similar to the observations for the formation of Ag nanoparticles. As the concentration of Au(III) solution was further diluted, the Au nanoparticles became smaller (<1 nm; see Supporting Information).

To see if the same gold nanoparticles could be formed only by the Ni(II) macrocyclic complex, solid [Ni(cyclam)(2-naphthalenecarboxylate)$_2$] (0.045 g, 0.067 mmol) was immersed in the EtOH solution (5 mL) of NaAuCl$_4$·2H$_2$O (1.7×10^{-2} M, 0.086 mmol) for 5 min. A brown solid resulted whose EPR spectrum ($g_\perp = 2.174$ and $g_\parallel = 2.018$) indicated the presence of Ni(III) species, and the TEM images showed the formation of much bigger Au nanoparticles (10–100 nm) compared to those produced by the present host solid.

The XRPD patterns (Figure 10) show that all peaks corresponding to the host framework are retained, even after the formation of Au nanoparticles of 2 nm by immersion of **1** in the NaAuCl$_4$ solution for 5 min to 46 h. The peaks corresponding to gold nanoparticles appear at $2\theta = 38.1°$ and $44.2°$,[46] even

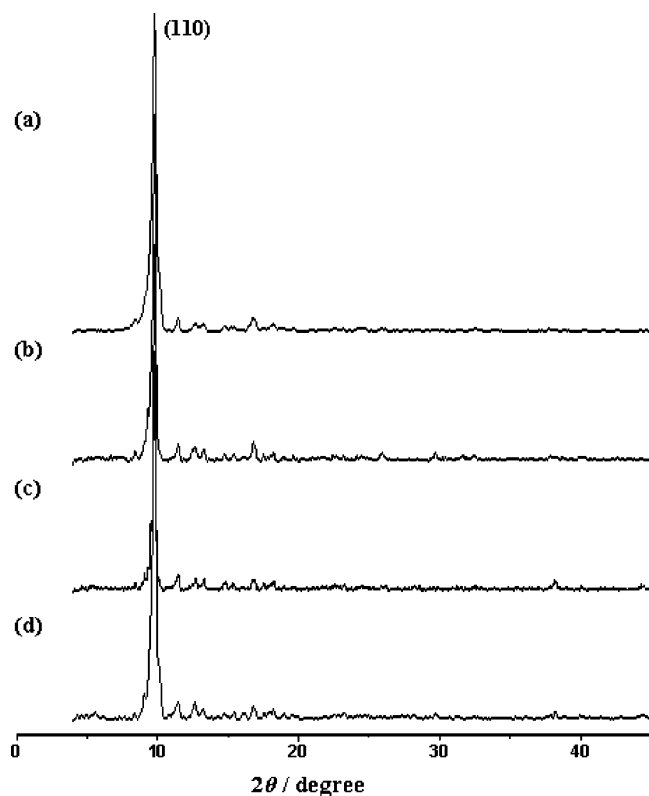(46) Sarma, T. K.; Chowdhury, D.; Paul, A.; Chattopadhyay, A. *Chem. Commun.* **2002**, 1048–1049.

Figure 10. XRPD patterns for (a) original host framework **1**, (b) solid isolated after immersion in the EtOH solution of $NaAuCl_4$ (3.4×10^{-2} M) for 5 min, (c) solid isolated after immersion for 20 min, and (d) solid isolated after immersion for 46 h.

though the intensities are very weak. The elemental analysis data (see Experimental Section) indicate that a stoichiometric amount of Au nanoparticles ($Ni^{II}:Au^{III} = 3:1$) was formed by the redox reaction between host solid and Au(III) ions, which resulted in a positively charged network incorporating Ni(III) ions and Cl^- inclusions. Similarly to the formation of Ag nanoparticles, the results again suggest that Au(III) metal ions were introduced between the layers, reacted with the Ni(II) species incorporated in the host layer, and were then reduced to Au(0) atoms, which diffused to the surface of the host to aggregate to nanoparticles.

Previously, we reported the production of Ag nanoparticles (3 nm) by immersion of the host framework having one-dimensional (1D) channels (aperture size, 0.73 nm), which was constructed by the packing of linear coordination polymer chains, in the MeOH solution of $AgNO_3$.[18] In this case also, the host framework was retained even after formation of Ag nanoparticles (by 10 min of immersion) that were much bigger than the aperture size of the 1D channels, although the structure was eventually altered after 18 h of immersion in the $AgNO_3$ solution. It was also reported that nanoparticles of Pd(0) of 1.4 nm, Cu(0) of 3−4 nm, and Au(0) of 5−20 nm were produced when metal precursor complexes were introduced into the 3D channels (pore size, 0.8 nm) of MOF-5 and then reduced with H_2 gas.[47] The XRPDs indicate that the MOF-5 framework was destroyed in the case of Pd nanoparticles, but the framework structure was retained after the formation of Cu and Au
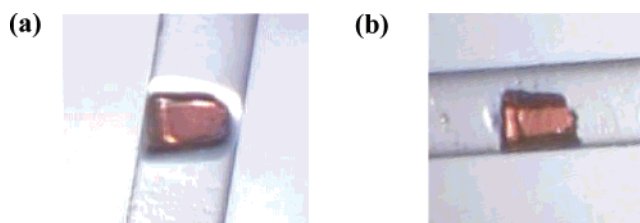

Figure 11. Photographs for (a) original crystal **1** with mother liquor and (b) desolvated crystal **2**, which was prepared by transferring the same crystal **1** of (a) to other capillary tube and then heating it at 180 °C under 10^{-5} Torr for 24 h.

nanoparticles. Although there is no proposed mechanism to explain how metal nanoparticles that are much bigger (2−25 times) than the pore size of MOF-5 formed and how they grew, we may assume that Pd atoms form and grow to nanoparticles within the channels of MOF-5, but Cu and Au atoms form in the channel and then migrate to the surface of the solid to aggregate into nanoparticles. In zeolites cases also,[48,49] nanoparticles or clusters that were much bigger than the pore size of the zeolites formed when the precursor complexes were introduced into the pores and then reduction processes were followed, and whether the particles grew on the surface or within the pores was proposed on the basis of the XRPD or EXAFS data. It seems that both the type of network and the identity of metal nanoparticles determine the retention or deterioration of the framework structure on formation of metal nanoparticles.

Single-Crystal-to-Single-Crystal Transformation on Guest Removal. When crystal **1** was heated at 180 °C under 10^{-5} Torr for 24 h, guest water molecules in **1** were completely removed to yield desolvated solid $\{[Ni(cyclam)]_2[BPTC]\}_n$ (**2**). During this process, the single crystallinity was retained intact (Figure 11), and the X-ray structure of **2** was determined. The N_2 gas sorption data measured for **2** indicated that it was nonporous.

The X-ray crystal structure of **2** is shown in Figure 12. The cell parameters, including the cell volume of **2**, changed slightly compared with those of **1** (Table 1). However, the X-ray data quality of **2** is as good as that of **1**. The overall 2D network structure of **2** is similar to that of **1**. The square grids extend parallel to the (110) plane. The dihedral angle between the two phenyl rings of $BPTC^{4-}$ and the Ni··Ni distances within the layer are almost same as those of **1** (Table 2). In addition, the different chirality of each square compartment that results in the achiral 2D layer and the stacking of 2D grids in the staggered manner are also the same as in **1**. However, significant rearrangements of the molecular components occur on removal of the water guest molecules that are intercalated between the layers. In Figure 12c, the ORTEP drawings of **1** and **2** are compared by superimposing all the corresponding Ni atoms at the same positions, since all Ni atom positions of **2** are retained the same as in **1** in the crystallographic data. On removal of the water guest molecules, the carboxylate planes rotate along the C(phenyl)··C(carboxylate) axis. The macrocyclic rings in **2** also rotate relative to the original positions since N−H of the macrocycle is hydrogen-bonded with the oxygen atom of the noncoordinating carbonyl group. Moreover, Ni−N_4 macrocyclic planes exhibit a bending motion relative to the Ni−O bond axes

(47) Hermes, S.; Schroter, M.-K.; Schmid, R.; Khodeir, L.; Muhler, M.; Tissler, A.; Fischer, R. W.; Fischer, R. A. *Angew. Chem., Int. Ed.* **2005**, *44*, 6237−6241.

(48) Plyuto, Y.; Berquier, J.-M.; Jacquiod, C.; Ricolleau, C. *Chem. Commun.* **1999**, 1653−1654.

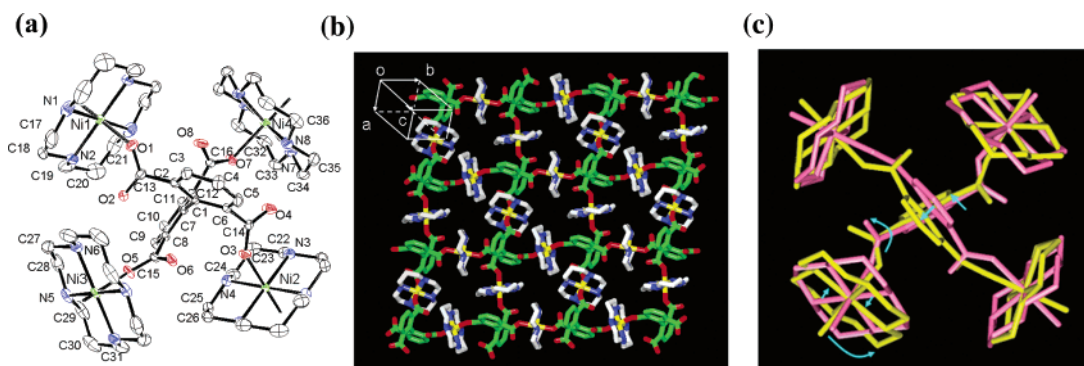(49) Li, F.; Gates, B. C. *J. Phys. Chem. B* **2003**, *107*, 11589−11596.

Figure 12. X-ray crystal structure of {[Ni(cyclam)]₂[BPTC]}ₙ (**2**). (a) An ORTEP drawing with atomic numbering scheme. The thermal ellipsoids are drawn with 30% probability. (b) Top view seen on the (110) plane, showing a 2D square-grid. Color scheme is the same as in Figure 1. (c) Comparison of the X-ray structures of **1** (pink) and **2** (yellow) with all corresponding Ni(II) positions in **1** and **2** superimposed.

Table 2. Selected Distances (Å) and Dihedral Angles (deg)[a] of **1** and **2**

	1	2		1	2
Ni1···Ni2	10.358(1)	10.173(1)	Ni1···Ni3	7.375(0)	7.308(1)
Ni3···Ni4	10.998(1)	11.047(1)	Ni1···Ni4	7.728(0)	7.704(1)
Ni1···Ni2($-x + 2, -y, -z$)	10.998(1)	11.047(1)	Ni2···Ni3	7.728(0)	7.704(1)
Ni3···Ni4($-x + 2, -y, -z + 1$)	10.358(1)	10.173(1)	Ni2···Ni4	7.375(0)	7.308(1)
∠Ph1−Ph2	78.1(2)	79.2(1)	∠Ni1−Ni3	76.6(2)	83.3(2)
∠Ph1−C13	61.0(5)	49.8(4)	∠Ni1−Ni4	66.0(2)	86.7(2)
∠Ph1−C14	41.8(3)	77.0(3)	∠Ni2−Ni3	87.2(2)	68.1(2)
∠Ph2−C15	55.6(4)	27.9(6)	∠Ni2−Ni4	87.3(2)	76.1(2)
∠Ph2−C16	28.2(7)	48.5(6)	∠Ni1−Ni2	62.4(2)	70.9(2)
∠Ph1−Ni1	75.4(2)	61.4(2)	∠Ni3−Ni4	46.1(3)	43.0(2)
∠Ph1−Ni2	57.3(2)	73.4(2)	∠C13−Ni1	85.0(4)	61.5(3)
∠Ph2−Ni3	78.7(2)	65.3(2)	∠C14−Ni2	60.6(6)	82.9(5)
∠Ph2−Ni4	64.1(2)	79.5(1)	∠C15−Ni3	78.9(5)	70.6(3)
			∠C16−Ni4	69.6(6)	75.4(5)

[a] The dihedral angles between two least-squares planes involving the noted atoms, as indicated below.
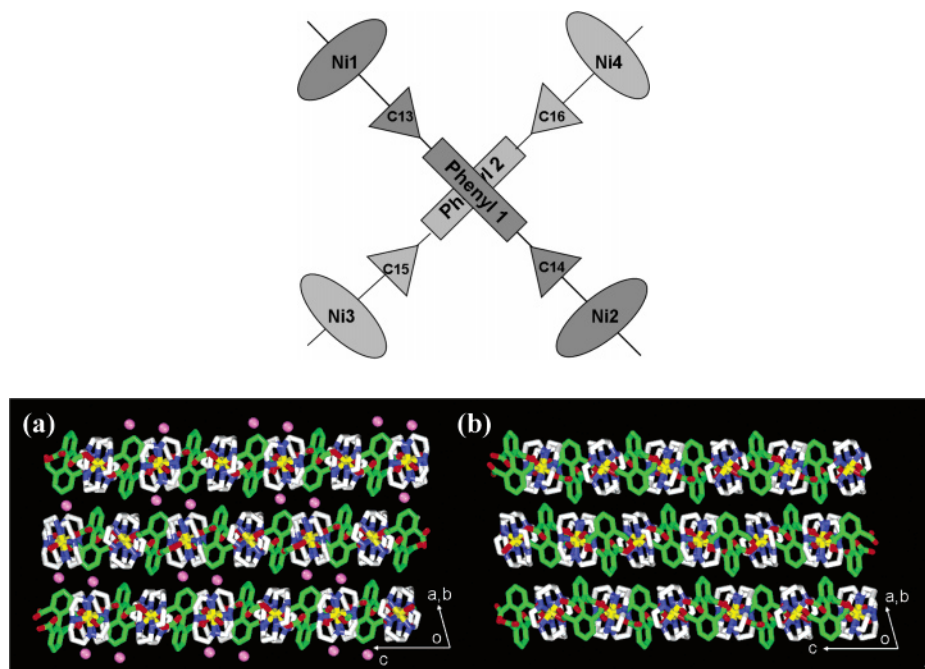

Figure 13. Side views for stacked square-grid networks: (a) **1** and (b) **2**.

with retention of the Ni coordinates and N−H···O hydrogen bonds. The axis linking C4··C1−C7··C10 atoms of phenyl rings of BPTC⁴⁻ units shifts by 18.3° relative to the (110) plane, since the dihedral angles between the (110) plane where Ni1, Ni2, Ni3, and Ni4 atoms locate and the line linking C4··C1−C7··C10 are 97.2° for **1** and 78.9° for **2** (Figure 13). Therefore, the

motion of the biphenyl group on desolvation can be considered as a swing. These extensive harmonic motions give rise to significant changes in the dihedral angles between the phenyl ring and the related carboxylate planes as well as the dihedral angles between the macrocyclic ring planes, as summarized in Table 2.
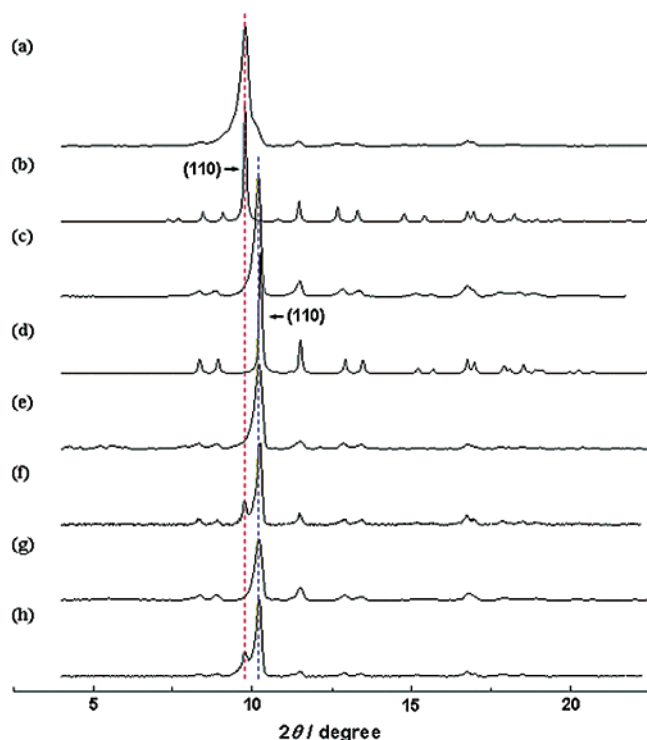
Figure 14. XRPD patterns for (a) original solid **1**, (b) simulated pattern for **1** based on the X-ray single-crystal data, (c) desolvated solid **2** prepared by heating **1** at 210 °C for 10 h, (d) simulated pattern for the desolvated solid based on the X-ray single-crystal data of **2**, (e) solid isolated after desolvated solid **2** was immersed in water for 3 h, (f) solid isolated after desolvated solid **2** was immersed in water for 4 days, (g) solid after desolvated solid **2** was exposed to water vapor for 1 day, and (h) solid after desolvated solid **2** was exposed to water vapor for 4 days.

The XRPD patterns (Figure 14) indicate that the peak at $2\theta = 9.7°$ for **1**, corresponding to the (110) plane, shifts to a higher angle ($2\theta = 10.2°$) in **2**. This shift corresponds to reduction of the interlayer distance on guest removal by 0.42 Å, from 9.03 to 8.61 Å, according to the Bragg equation. The void volume of **2** is 7.8% of the total crystal volume, as estimated by using PLATON,[33] based on the single-crystal X-ray structure. When crystal **2** was immersed in water for 3 h or exposed to water vapor for 1 day, the XRPD of **2** did not change. In the organic solvents, such as benzene, chloroform, and EtOH, the XRPD of **2** did not change either (see Supporting Information). However, when crystal **2** was immersed in water or exposed to water vapor for 4 days, the (110) peak of the original structure started to be restored, although its intensity was remarkably weaker than that of the peak of the dehydrated structure. It seems that diffusion of water molecules into the present dehydrated nonporous structure is extremely slow. This is contrary to the report on the nonporous calixarene crystal that adsorbs guest

organic solvent molecules very rapidly (within 15 min) via the extensive movement of molecular components in the crystal.[50]

Crystal dynamics such as spongelike shrinkage/swelling,[6,23] sliding,[20,21] swing,[25] or rotational motions[19] were independently reported previously. However, single-crystal-to-single-crystal transformation involving various types of motions (rotation, swing, and bending) as in the present crystal, which gives rise to the reduction of the interlayer distance on desolvation, has never been observed.

In conclusion, a 2D square-grid coordination polymer, $\{[Ni(cyclam)]_2[BPTC]\}_n \cdot 2nH_2O$ (**1**), which is assembled from $[Ni(cyclam)]^{2+}$ and 1,1′-biphenyl-2,2′,6,6′-tetracarboxylate ($BPTC^{4-}$), is redox-active and produces Ag (ca. 4 nm) and Au (ca. 2 nm) nanoparticles at room temperature simply on immersion of the solid in the EtOH solutions of $AgNO_3$ and $NaAuCl_4 \cdot 2H_2O$, respectively. On the basis of the elemental analysis data indicating stoichiometric redox reaction of Ag(I)/Au(III) ions with Ni(II) species of **1** and the XRPD patterns showing retention of the framework structure, as well as the EPR and XPS data, we suggest that Ag(I)/Au(III) ions are intercalated between the host layers and react with the Ni(II) species incorporated in the host to form metal(0) atoms, which diffuse to the surface of the solid to grow into the nanoparticles. Solid **1** shows novel crystal dynamics on guest water removal, with retention of the single crystallinity. Comparison of the X-ray crystal structures of **1** and its desolvated solid **2** reveals extensive motions of the molecular components in response to guest removal involving rotation, swing, and bending motions, which gives rise to the reduction of interlayer distance.

Supporting Information Available: TGA/DSC trace of **1**, EDS data for Ag(0) and Au(0) nanocomposites with host solid **1**, N_2 gas sorption data for **2**, TEM images for Ag and Au nanoparticles obtained under various experimental conditions, XRPD patterns of **2** measured after immersion in various organic solvents, tables summarizing the various experimental conditions and the size of Ag and Au nanoparticles formed, and tables of X-ray crystal data for **1** and **2** (PDF). X-ray crystallographic files (CIF). This material is available free of charge via the Internet at http://pubs.acs.org.

JA056963L

(50) Atwood, J. L.; Barbour, L. J.; Jerga, A.; Schottel, B. L. *Science* **2002**, *298*, 1000−1002.